

Coalescence of a bubble at a fluid–fluid interface: Comparison of theory and experiment

Kai-Bin Fu^{a,b}, John C. Slattery^{a,*}

^a Department of Aerospace Engineering, Texas A&M University, College Station, TX 77843-3141, USA

^b Department of Mathematics, Texas A&M University, College Station, TX 77843-3141, USA

Received 25 August 2006; accepted 13 June 2007

Available online 30 June 2007

Abstract

Coalescence times for air bubbles rising through hexadecane to an air–hexadecane interface are measured and compared with an analysis based upon our previous extension of continuum mechanics to the nanoscale [J.C. Slattery, E.-S. Oh, K. Fu, Chem. Eng. Sci. 59 (2004) 4621–4635] with the assumption of retarded dispersion forces. The relation between the retarded and non-retarded Hamaker constants proposed by Görner and Pich [J. Aerosol Sci. 20 (7) (1989) 735–747] is tested for the first time.

© 2007 Elsevier Inc. All rights reserved.

Keywords: Coalescence time; Retarded Hamaker constant; Dispersion forces; Van der Waals forces; Nanoscale mechanics

1. Introduction

Coalescence plays a crucial role in many industrial processes. The rate at which drops or bubbles, suspended in a liquid, coalesce is important to the preparation and stability of emulsions, of foams, and of dispersions; to liquid–liquid extractions; to the formation of an oil bank during the displacement of oil from a reservoir rock; to mineral flotation.

Usually, coalescence can be thought of as occurring in three stages:

- (1) approach of one drop or bubble toward another or a fluid–fluid interface,
- (2) formation of a fluid film of the continuous phase,
- (3) thinning and rupture of the thin film.

Recent reviews of coalescence have been given by Leal [1] and Slattery et al. [2, Section 3.3.3]. In what follows, we will focus on the more restricted problem of coalescence as a drop or

bubble approaches an extended interface, emphasizing the deformation of the thin film as rupture is approached.

Hahn and Slattery [3] have followed Lin and Slattery [4] and Hahn et al. [5] in constructing a more complete analysis for the effects of the surface viscosities upon the coalescence time. Their qualitative conclusions are the same as those of Hahn and Slattery [6] described above, but they observe that the neglect of film dimpling by Hahn and Slattery [6] leads to serious errors. This is consistent with the better agreement found between the computations of Hahn and Slattery [3] and the experimental observations of Li and Slattery [7]. Li [8,9] had extended the model of Hahn et al. [5] to study the effects of surface tension, surface viscosity, surface diffusion and London–van der Waals forces on coalescence.

1.1. Introduction: Views or models of the interface

How we correct for the effects of the long-range intermolecular forces depends upon our view or model of the interfacial region. Expanding upon the discussion of Slattery et al. [2,10] identify six views or models of the interfacial region, each having its own somewhat different notation.

* Corresponding author. Professor of Aerospace Engineering and of Mathematics. Fax: +1 979 845 6051.

E-mail address: slattery@tamu.edu (J.C. Slattery).

(i) The most realistic view of an interface is as a thin, three-dimensional region. There is a smooth transition of the material's density and stress-deformation behavior through this interfacial region from one phase to the other. Because it is so thin, it is extremely difficult to study experimentally the material's behavior in the interfacial region, except as the critical point is approached [11–15]. With this point of view, $\rho^{(I)}$, $\mathbf{v}^{(I)}$ and $\mathbf{T}^{(I)}$ denote the true interfacial density, velocity and stress tensor in the interfacial region.

(ii) In the second view or model, we recognize that, since we have no way of knowing the true material behavior of the interfacial region, we will use bulk descriptions of material behavior corrected for the effects of long-range intermolecular forces from the adjacent phases. By $\rho^{(I,\text{bulk})}$, $\mathbf{v}^{(I,\text{bulk})}$ and $\mathbf{T}^{(I,\text{bulk})}$, we indicate the density, velocity and stress tensor observed in the interfacial region (I) using bulk descriptions for interfacial behavior.

Note that, with this point of view, the interface is three-dimensional as in view (i). Consistent with view (i), $\mathbf{T}^{(I,\text{bulk})}$ is a continuous function of position in passing from the interfacial region to the bulk material.

For the sake of simplicity and clarity, we focus on quasi-static systems and ignore effects of gravity. With this point of view, the differential momentum balance reduces to

$$\text{div } \mathbf{T}^{(I,\text{bulk})} + \mathbf{b}^{(\text{corr})} = 0, \quad (1)$$

where $\mathbf{b}^{(\text{corr})}$ is the body force per unit volume introduced to correct for the use of bulk material behavior in the interfacial region.

In order to illustrate the estimation of $\mathbf{b}^{(\text{corr})}$, consider the two cases shown in Fig. 1.

(a) For the two phases shown in Fig. 1a, in estimating $\mathbf{b}^{(A,\text{corr})}$ we will

- subtract the force per unit volume at a point in phase A attributable to that portion of phase A that has been replaced by phase B, and
- add the force per unit volume at this same point in phase A attributable to phase B.

In reality, the effective replacement region $R^{(B)}$ may be no more than 100 nm thick, since outside this region the intermolecular forces between phases A and B go to zero.

(b) Let us now consider the thin film as shown in Fig. 1b. In order to estimate $\mathbf{b}^{(A,\text{corr})}$, we will

- subtract the force per unit volume at a point in phase A attributable to that portion of phase A that has been replaced by phase C and phase B,
- add force per unit volume at this same point in phase A attributable to phase C, and
- add force per unit volume at this point in phase A attributable to phase B.

For more about view (ii) and how it can be applied, see Slattery et al. [2, Section 3.3.1].

(iii) In the third view or model, the interfacial region is described by a two-dimensional dividing surface. The effects of long-range intermolecular forces are taken into account by introducing *excess quantities*, such as a surface tension or energy γ , in the dividing surface [2, Sections 1.3.5 and 2.1.6]. The dividing surface now becomes a two-dimensional representation of the interface.

Ignoring inertial forces and gravity (for example), the differential and jump momentum balances become [2, Section 2.2.1, Appendix B]

$$\text{div } \mathbf{T} = 0, \quad (2)$$

$$\nabla_{(\sigma)} \gamma + 2H\gamma\xi + [\mathbf{T}\xi] = 0, \quad (3)$$

where $\nabla_{(\sigma)}$ denotes a surface gradient, γ is the surface tension, H is the mean curvature of the dividing surface, and ξ the unit normal to the dividing surface Σ . The boldface brackets denote the jump of the quantity enclosed across the interface between phases A and C:

$$[A\xi] \equiv A^{(A)}\xi^{(A)} + A^{(C)}\xi^{(C)}, \quad (4)$$

where $\xi^{(i)}$ is the unit normal to the interface pointing into phase i . By ρ , \mathbf{v} and \mathbf{T} we mean the density, velocity, and stress tensor determined using bulk descriptions of material behavior and excess properties such as γ in the dividing surface to correct for long-range intermolecular forces rather than $\mathbf{b}^{(\text{corr})}$.

Note that the view inherently assumes that all effects of long-range intermolecular forces from the adjacent phase are incorporated in the surface tension or energy γ . By \mathbf{T} we mean that the stress that would be observed with no further correction for long-range intermolecular forces.

(iv) The fourth view or model is again view (iii), in which one enforces consistency with view (ii). Comparing (1) and (2) and observing that [2, Section 2.2.2]

$$\mathbf{b}^{(\text{corr})} = -\nabla\phi^{(\text{corr})} \quad (5)$$

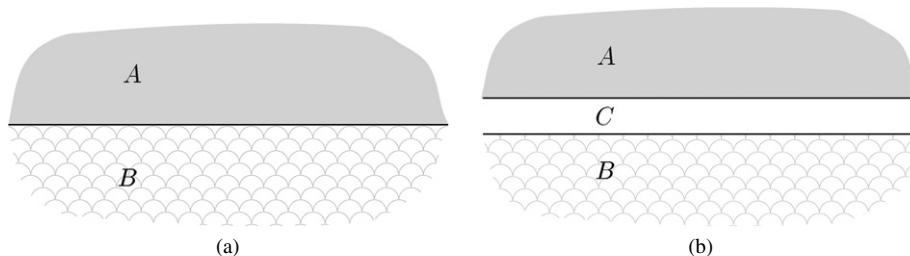


Fig. 1. For simplicity, the dividing surfaces and the two singular surfaces for each interface are shown as a single curve. Two cases are illustrated. (a) Two semi-infinite phases A and B. (b) Two semi-infinite phases A and B separated by a thin film of phase C.

we conclude that [10]

$$\mathbf{T} = \mathbf{T}^{(I, \text{bulk})} - \Phi^{(\text{corr})} \mathbf{I}. \quad (6)$$

This means that the differential momentum balance takes the form

$$\begin{aligned} \text{div } \mathbf{T} &= 0, \\ \text{div}(\mathbf{T}^{(I, \text{bulk})} - \Phi^{(\text{corr})} \mathbf{I}) &= 0, \end{aligned} \quad (7)$$

and that the jump momentum balance becomes

$$\begin{aligned} \nabla_{(\sigma)} \gamma + 2H\gamma\xi + [\mathbf{T}\xi] &= 0, \\ \nabla_{(\sigma)} \gamma + 2H\gamma\xi + [(\mathbf{T}^{(I, \text{bulk})} - \Phi^{(\text{corr})} \mathbf{I})\xi] &= 0. \end{aligned} \quad (8)$$

Slattery et al. [2, Section 2.2.2] conclude that

$$\gamma \equiv \int_0^\infty \Phi^{(A, \text{corr})} d\lambda + \int_{-\infty}^{-\delta^{(AB)}} \Phi^{(B, \text{corr})} d\lambda. \quad (9)$$

For more about view (iv) and how it can be applied, see Slattery et al. [2, Section 3.3].

- (v) As Slattery et al. [2, Sections 2.2.6 and 2.2.7] explain, this model is most easily understood as a derivative of view (ii). The effect of long-range intermolecular forces is partially accounted for by introducing a dividing surface and a surface tension or energy γ^∞ , the interfacial tension observed for a single interface with unbounded adjoining phases. The remainder of the effect is taken into account with a body force correction per unit volume [2, Section 2.2.7]

$$\mathbf{b}^{(\text{corr})\infty} = -\nabla \Phi^{(\text{corr})\infty}. \quad (10)$$

We conclude that the differential momentum balance takes the form

$$\text{div}(\mathbf{T}^{(I, \text{bulk})\infty} - \Phi^{(\text{corr})\infty} \mathbf{I}) = 0 \quad (11)$$

and that the jump momentum balance becomes

$$\nabla_{(\sigma)} \gamma^\infty + 2H\gamma^\infty \xi + [\mathbf{T}^{(I, \text{bulk})\infty} \xi] = 0. \quad (12)$$

For more on this point of view and how it can be applied, see Slattery et al. [2, Sections 2.2.3 and 3.3].

- (vi) The sixth view or model is similar to view (iii), but all excess properties such as γ are determined empirically.

1.2. Retarded dispersion forces

Intermolecular forces can be categorized as either short-range (electrostatic and steric repulsion) or long-range (gravitational, electrostatic, and dispersion). We will focus on dispersion forces, which are also known as dispersion forces between neutral molecules, van der Waals dispersion forces, “London forces, charge-fluctuation forces, electrodynamic forces, and induced-dipole–induced-dipole forces” [16, p. 83]. Interesting reviews of dispersion forces have been given by Israelachvili [16] and by Bowen and Jenner [17].

If r is the intermolecular distance, the intermolecular potential for dispersion forces is inversely proportional to r^6 for $r < 5$ nm. But for $r > 5$ nm, one should expect the dispersion

forces to be retarded [16, pp. 197–198]. Retardation occurs, where the intermolecular distance is sufficiently large that the time required for the electric field of one dipole to reach a second and return is comparable to the period of the fluctuating dipole [16, p. 106]. Because the critical film thicknesses (the film thickness at which an instability develops resulting in coalescence) measured or predicted by Allan et al. [18], MacKay and Mason [19], Vrij [20], Ivanov et al. [21], Burrill and Woods [22], and Chen et al. [23] are typically larger than 12 nm, we expect that the point-to-point forces are retarded.

Casimir and Polder [24] were the first ones to describe retarded dispersion forces with a monotonically decreasing function of r . But two different approaches developed.

Russel et al. [25] and Mahanty and Ninham [26] still assumed that the intermolecular force potential was inversely proportional to r^6 , but they recognized that the proportionality factor was a monotonically decreasing function of r [25, p. 154]. This has the distinct advantage that the dispersion force potential varies smoothly as a function of r between the retarded and non-retarded cases.

Following Casimir and Polder [24], Zimon [27] and Görner and Pich [28] recommended force potentials for retarded dispersion forces that are inversely proportional to r^7 , in which the retarded Hamaker constant B is not a function of r . Although such force potentials do not vary smoothly between the retarded and non-retarded cases, they are easier to implement, if one is concerned only with the retarded case as in coalescence. Görner and Pich [28] employed the retardation correction function of Overbeek [29] and derived the relation between retarded (B) and non-retarded (A) Hamaker constants

$$B = \frac{2.45\lambda_L A}{40\pi^2}. \quad (13)$$

Here λ_L is introduced as the “London wavelength” without a further definition. We will say more about this in our conclusions.

In what following, we will adopt view (v) discussed in Section 1.1. Retarded intermolecular forces have been incorporated into the computation for coalescence time of air bubbles rising through n -hexadecane. In the process, the retarded Hamaker constant becomes an adjustable parameter.

1.3. Correction potential $\Phi^{(\text{corr})\infty}$ for view (v) with retardation effect

Let us assume that the thin film shown in Fig. 2 is bounded by parallel planes; its thickness is the difference between h_1 and h_2 . Slattery et al. [2, Section 2.2.7] show that in region A

$$\Phi^{(A, \text{corr})\infty} = -\frac{B^{(ACB)} - B^{(AC)} + B^{(CC)} - B^{(BC)}}{10\pi(z_2 - h_2)^4} \quad (14)$$

and in region B

$$\Phi^{(B, \text{corr})\infty} = \frac{B^{(BC)} - B^{(ACB)} - B^{(CC)} + B^{(AC)}}{10\pi(h_1 - z_2)^4} \quad (15)$$

and in region C

$$\Phi^{(C, \text{corr})\infty} = 0. \quad (16)$$

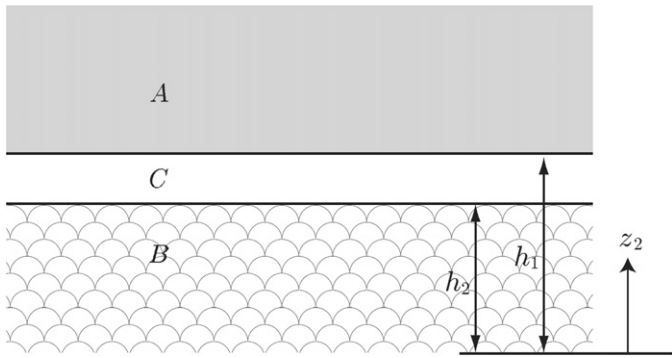


Fig. 2. A thin film bounded by two parallel, plane interfaces.

Here $B^{(ACB)}$ denotes the effective, Lifshitz type, retarded Hamaker constant [17] for species A and B interacting across an intermediate phase C . If there is no intermediate phase or the intermediate phase is a vacuum, we use the notation $B^{(AB)}$.

2. Analysis

In what follows, we will focus on coalescence as a drop or bubble approaches an extended interface, emphasizing the deformation of the thin film as rupture is approached. We will conclude with a comparison of our simulation with the results of a new experimental study of coalescence time, the time that a bubble appears to sit at an interface before the film ruptures and the bubble disappears. While the literature describes many experiments, to our knowledge none is suitable for testing our theory.

Fig. 3 shows the liquid film formed as a small drop or bubble approaches a fluid–fluid interface. Our objective is to determine the shape of this film as it drains with time. The solution that follows is a variation on that given by [4,5], now explained in the context of view (v) of Section 1.1.

In carrying out this computation, we will make a number of assumptions.

- (i) Viewed in the cylindrical coordinate system of Fig. 3, the two interfaces bounding the draining liquid film are axisymmetric ($i = 1, 2$):

$$z = h_i(r, t). \tag{17}$$

- (ii) The dependence of h_i ($i = 1, 2$) upon r is sufficiently weak that

$$\left(\frac{\partial h_i}{\partial r}\right)^2 \ll 1. \tag{18}$$

- (iii) Introducing

$$h = h(r, t) \equiv h_1 - h_2, \tag{19}$$

let R be the rim radius of the drop such that

$$\text{at } r = R = R(t) : \quad \frac{\partial h}{\partial r} = 0. \tag{20}$$

The Reynolds lubrication theory approximation applies in the sense that, if

$$h_0 \equiv h(0, 0) \tag{21}$$

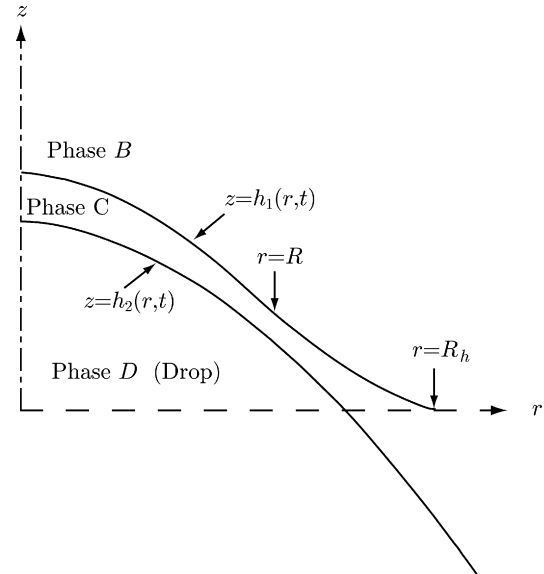


Fig. 3. A symmetric drop or bubble (phase D) moves through a liquid (phase C) as it approaches a fluid–fluid interface (between phases C and B). The configuration of the drop–fluid interface is given by $z = h_2(r, t)$; that of the fluid–fluid interface by $z = h_1(r, t)$.

and

$$R_0 \equiv R(0) \tag{22}$$

we will require

$$\left(\frac{h_0}{R_0}\right)^2 \ll 1. \tag{23}$$

- (iv) There is surfactant present in both interfaces. The resulting interfacial tension gradients are sufficiently large that the tangential components of velocity \mathbf{v} are zero ($i = 1, 2$)

$$\text{at } z = h_i : \quad \mathbf{P} \cdot \mathbf{v} = 0. \tag{24}$$

Here \mathbf{P} is the projection tensor that transforms every vector on an interface into its tangential components. The interfacial tension gradient required to create such an immobile interface is very small [4,5,30,31]. We will consequently assume that at the same radial positions the interfacial tensions in the two interfaces are equal. In this limit, the results developed will apply both to a liquid drop approaching a liquid–liquid interface and to a gas bubble approaching a gas–liquid interface, since all circulation within phases B and D in Fig. 3 is suppressed.

- (v) The effect of mass transfer is neglected.
- (vi) The pressure p_0 within phase B , the drop or bubble, is independent of time and position. The pressure within phase A is equal to the local hydrostatic pressure p_h , which is also assumed to be a constant.
- (vii) Phase C is an incompressible, Newtonian fluid, the viscosity of which is a constant.
- (viii) All inertial effects are neglected.
- (ix) The effects of gravity and of electrostatic double-layer forces are neglected within the draining film, although of

course the bubble itself rises as the result of gravitational forces.

- (x) The pressure within the draining film approaches its local hydrostatic value beyond the rim where the Reynolds lubrication theory approximation (assumption (iii)) is still valid. At this point, ($r = R_h$), the two principal curvatures of the drop are constants independent of time,

$$\text{at } r = R_h: \quad \frac{\partial h}{\partial r} = \left(\frac{\partial h}{\partial r} \right)_{t=0}, \quad (25)$$

$$\text{at } r = R_h: \quad \frac{\partial^2 h}{\partial r^2} = \left(\frac{\partial^2 h}{\partial r^2} \right)_{t=0}. \quad (26)$$

- (xi) Experimental observations [18,32] suggest that there is a time at which the thinning rate at the rim is equal to the thinning rate at the center. At time $t = 0$ in our computations, the thinning rate is independent of radial position. For $t > 0$, the thinning rate at the center is always less than the thinning rate at the rim as the result of long-range intermolecular forces.
- (xii) The drop is sufficiently small that it may be assumed to be spherical. This is equivalent to assuming that the Bond number

$$N_{Bo} \equiv \frac{\Delta \rho g R_b^2}{\gamma^\infty} \ll 1. \quad (27)$$

Here

$$\Delta \rho \equiv \rho^{(D)} - \rho^{(C)} \quad (28)$$

is the magnitude of the density difference between the drop or bubble phase D and the continuous phase C , g the magnitude of the acceleration of the gravity, R_b the radius of the drop, and γ^∞ the equilibrium interfacial tension.

- (xiii) Within each phase, the correction for long-range intermolecular forces is taken from Slattery et al. [10] and Oh et al. [33].
- (xiv) Because the critical film thicknesses measured or predicted by Allan et al. [18], MacKay and Mason [19], Vrij [20], Ivanov et al. [21], Burrill and Woods [22], and Chen et al. [23] are typically larger than 12 nm, we expect that the point-to-point forces are retarded.
- (xv) In discussion the thin liquid film formed in the neighborhood of the common line, we will employ view (v) of Section 1.1. The correction for long-range intermolecular forces from the adjacent phases will be taken from Slattery et al. [2, Section 2.2]. We will consider neither steric forces nor perturbations to the correction for intermolecular forces attributable to trace amounts of surfactants.

In constructing this development, we will find it convenient to work in terms of these dimensionless variables:

$$\begin{aligned} r^* &\equiv \frac{r}{R_0}, & z^* &\equiv \frac{z}{h_0}, & h_i^* &\equiv \frac{h_i}{h_0}, & H_i^* &\equiv H_i R_0 \quad (i = 1, 2), \\ h^* &\equiv h_1^* - h_2^*, & p^* &\equiv \frac{p^{(C)}}{\rho^{(C)} v_0^2}, & p_0^* &\equiv \frac{p_0}{\rho^{(C)} v_0^2}, \\ p_h^* &\equiv \frac{p_h}{\rho^{(C)} v_0^2}, & v_r^* &\equiv \frac{v_r}{v_0}, & v_z^* &\equiv \frac{R_0 v_z}{h_0 v_0}, \\ t^* &\equiv \frac{t v_0}{R_0}, & \gamma^* &\equiv \frac{\gamma}{\gamma^\infty}, \\ \Phi^{(i,\text{corr})\infty*} &\equiv \frac{\Phi^{(i,\text{corr})\infty}}{\rho^{(C)} v_0^2}, & \mathcal{P}^* &\equiv \frac{p^{(C)} + \Phi^{(C,\text{corr})\infty}}{\rho^{(C)} v_0^2}, \\ \mathcal{P}_0^* &\equiv \frac{p_0 + \Phi^{(B,\text{corr})\infty}}{\rho^{(C)} v_0^2}, & \mathcal{P}_h^* &\equiv \frac{p_h + \Phi^{(D,\text{corr})\infty}}{\rho^{(C)} v_0^2} \end{aligned} \quad (29)$$

and dimensionless Reynolds, Weber, and capillary numbers

$$\begin{aligned} N_{Re} &\equiv \frac{\rho^{(C)} v_0 R_0}{\mu}, & N_{We} &\equiv \frac{\rho^{(C)} v_0^2 R_0}{\gamma^\infty}, \\ N_{ca} &\equiv \frac{\mu v_0}{\gamma^\infty}. \end{aligned} \quad (30)$$

Here H_i ($i = 1, 2$) are the mean curvatures of the interfaces. The characteristic speed v_0 will be defined later.

Equation (17) suggests that we seek a solution in which the velocity distribution takes the form

$$\begin{aligned} v_r^* &= v_r^*(r^*, z^*, t^*), \\ v_z^* &= v_z^*(r^*, z^*, t^*), \\ v_\theta^* &= 0. \end{aligned} \quad (31)$$

Under these circumstances, the differential mass balance for an incompressible fluid requires [34, p. 50]

$$\frac{1}{r^*} \frac{\partial(r^* v_r^*)}{\partial r^*} + \frac{\partial v_z^*}{\partial z^*} = 0. \quad (32)$$

In the limit of assumptions (iii) and (viii), the r^* -, θ -, and z^* -components of the differential momentum balance for an incompressible, Newtonian fluid with a constant viscosity reduces for creeping flow to [34, p. 52]

$$\frac{\partial \mathcal{P}^*}{\partial r^*} = \frac{1}{N_{Re}} \left(\frac{R_0}{h_0} \right)^2 \frac{\partial^2 v_r^*}{\partial z^{*2}}, \quad (33)$$

$$\frac{\partial \mathcal{P}^*}{\partial \theta^*} = 0, \quad (34)$$

$$\frac{\partial \mathcal{P}^*}{\partial z^*} = \frac{1}{N_{Re}} \frac{\partial^2 v_z^*}{\partial z^{*2}}. \quad (35)$$

Here we have neglected the effects of gravity within the draining liquid film (assumption (ix)), and we have represented the correction for long-range intermolecular forces as described in assumption (xiii). Equations (33) and (35) imply

$$\frac{\partial \mathcal{P}^*}{\partial z^*} \ll \frac{\partial \mathcal{P}^*}{\partial r^*} \quad (36)$$

and the dependence of \mathcal{P}^* upon z^* can be neglected. Note that the scaling argument used to neglect inertial effects (assumption (viii)) in arriving at (33) and (35) is presumed not to be the one ultimately used here. For this reason, we will regard the

magnitude of N_{Re} and the definition of v_0 to be as yet unspecified.

The jump mass balance is satisfied identically, since we define the position of the dividing surface by choosing $\rho^{(\sigma)} = 0$ [35] and since the effect of mass transfer is neglected (assumption (v)). The jump mass balance for surfactant is not required here, since we assume that the interfacial tension gradient developed in the interface is so small that its effect and the effect of a concentration gradient developed in the interface can be neglected (assumption (iv)).

With assumptions (v) and (vi), the jump momentum balance for the interface between phases *B* and *C* reduces to

$$\nabla_{(\sigma)}\gamma + 2H_1\gamma\xi - (\mathbf{T} + p_h\mathbf{I}) \cdot \xi = 0. \quad (37)$$

Here ξ is the unit normal to the interface pointing out of the liquid film. Under the conditions of assumptions (ii) and (iii), the *r*- and *z*-components of (37) assume the forms at $z^* = h_1^*$

$$\begin{aligned} \frac{\partial\gamma^*}{\partial r^*} - 2\frac{h_0}{R_0}H_1^*\gamma^* \frac{\partial h_1^*}{\partial r^*} - N_{\text{We}}\frac{h_0}{R_0}(p^* - p_h^*) \frac{\partial h_1^*}{\partial r^*} \\ - N_{\text{ca}}\frac{R_0}{h_0} \frac{\partial v_r^*}{\partial z^*} = 0 \end{aligned} \quad (38)$$

and

$$\begin{aligned} \frac{h_0}{R_0} \frac{\partial h_1^*}{\partial r^*} \frac{\partial\gamma^*}{\partial r^*} + 2H_1^*\gamma^* + N_{\text{We}}(p^* - p_h^*) - 2N_{\text{ca}} \frac{\partial v_z^*}{\partial z^*} \\ + N_{\text{ca}} \frac{\partial v_r^*}{\partial z^*} \frac{\partial h_1^*}{\partial r^*} = 0. \end{aligned} \quad (39)$$

The θ -component is satisfied identically. Adding $(h_0/R_0)(\partial h_1^*/\partial r^*)$ times (39) to (38) and recognizing assumptions (ii) and (iii), we have

$$\text{at } z^* = h_1^*: \quad \frac{\partial\gamma^*}{\partial r^*} - N_{\text{ca}}\frac{R_0}{h_0} \frac{\partial v_r^*}{\partial z^*} = 0, \quad (40)$$

so that (38) implies¹

$$\text{at } z^* = h_1^*: \quad 2H_1^*\gamma^* + N_{\text{We}}(p^* - p_h^*) = 0. \quad (41)$$

In a similar fashion, we can also see that the jump momentum balance for the interface between phases *C* and *A* reduces to

$$\text{at } z^* = h_2^*: \quad \frac{\partial\gamma^*}{\partial r^*} + N_{\text{ca}}\frac{R_0}{h_0} \frac{\partial v_r^*}{\partial z^*} = 0, \quad (42)$$

$$\text{at } z^* = h_2^*: \quad 2H_2^*\gamma^* - N_{\text{We}}(p^* - p_0^*) = 0. \quad (43)$$

¹ In arriving at (40) and (41), it was not necessary to make any statement about the relative magnitudes of N_{ca} and N_{We} or the definition of v_0 . But some statement is necessary, in order to establish consistency with (39).

Substituting (40) into (39), we have

$$2H_1^*\gamma^* + N_{\text{We}}(p^* - p_h^*) + 2N_{\text{ca}}\left(\frac{\partial v_r^*}{\partial z^*} \frac{\partial h_1^*}{\partial r^*} - \frac{\partial v_z^*}{\partial z^*}\right) = 0.$$

It follows from (64), (65), and (68) that

$$|2H_1^*\gamma^*| \gg \left| 2N_{\text{ca}}\left(\frac{\partial v_r^*}{\partial z^*} \frac{\partial h_1^*}{\partial r^*} - \frac{\partial v_z^*}{\partial z^*}\right) \right|$$

in agreement with (41).

We will recognize assumptions iii and iv to say

$$\text{at } z^* = h_i^*: \quad v_r^* = 0 \quad (i = 1, 2) \quad (44)$$

and we will employ (40) and (42) to calculate the interfacial tension gradient required to create the immobile interfaces assumed here.

Since we neglect the effect of mass transfer on the velocity distribution (assumption (v)),

$$\text{at } z^* = h_i^*: \quad v_z^* = \frac{\partial h_i^*}{\partial t^*} + \frac{\partial h_i^*}{\partial r^*} v_r^* \quad (i = 1, 2). \quad (45)$$

Note that

$$\text{at } r^* = R^*: \quad \frac{\partial h^*}{\partial r^*} = 0, \quad (46)$$

$$\text{at } r^* = 0: \quad \frac{\partial h^*}{\partial r^*} = \frac{\partial h_1^*}{\partial r^*} = 0, \quad (47)$$

and

$$\text{at } r^* = 0: \quad \frac{\partial p^*}{\partial r^*} = \frac{\partial \mathcal{P}^*}{\partial r^*} = 0. \quad (48)$$

Equations (41), (43), and (48) together with assumptions (ii) and (iv) imply

$$\begin{aligned} \text{at } r^* = 0: \quad \frac{\partial(H_1^* - H_2^*)}{\partial r^*} = \frac{1}{2} \frac{h_0}{R_0} \left(-\frac{1}{r^{*2}} \frac{\partial h^*}{\partial r^*} \right. \\ \left. + \frac{1}{r^*} \frac{\partial^2 h^*}{\partial r^{*2}} + \frac{\partial^3 h^*}{\partial r^{*3}} \right) = 0. \end{aligned} \quad (49)$$

Solving for the third derivative and applying L'Hospital's rule shows us that

$$\text{at } r^* = 0: \quad \frac{\partial^3 h^*}{\partial r^{*3}} = 0 \quad (50)$$

or alternatively

$$\text{at } r^* = 0: \quad \frac{\partial^2 h^*}{\partial r^{*2}} = \frac{1}{r^*} \frac{\partial h^*}{\partial r^*}. \quad (51)$$

According to assumption (x), there is a point $r^* = R_h^* > R^*$ where the pressure p^* within the draining film approaches the local hydrostatic pressure in the neighborhood of the drop and the effects of the London–van der Waals force disappear,

$$\text{at } r^* \rightarrow R_h^*: \quad p^* \rightarrow p_h^*, \quad h_1^* \rightarrow 0. \quad (52)$$

Assumption (x) also requires that

$$\text{at } r^* = R_h^*: \quad \frac{\partial h^*}{\partial r^*} = \left(\frac{\partial h^*}{\partial r^*} \right)_{r^*=0}, \quad (53)$$

$$\text{at } r^* = R_h^*: \quad \frac{\partial^2 h^*}{\partial r^{*2}} = \left(\frac{\partial^2 h^*}{\partial r^{*2}} \right)_{r^*=0}. \quad (54)$$

The initial time is to be chosen by requiring (assumption (xi))

$$\text{at } t^* = 0: \quad \frac{\partial h^*}{\partial t^*} = \text{const.} \quad (55)$$

Since the drop is sufficiently small to be assumed spherical (assumption (xii)), the jump momentum balance requires

[see (43)]

$$p_h^* - p_0^* = -\frac{2}{N_{We} R_b^*}, \quad (56)$$

where R_b is the radius of the bubble or drop. Because surface tension is assumed to be nearly independent of position by assumption (iv), (42) implies that the effects of viscous forces can be neglected in the jump momentum balance (see preceding footnote).

An integral momentum balance for the drop requires (for more details, see [31])

$$N_{ca} \int_0^{R_b^*} (p^* - p_h^*) r^* dr^* = \frac{(R_0)^2 \Delta \rho g}{\gamma^\infty} \frac{2}{3} (R_b^*)^3. \quad (57)$$

If

$$R_f \equiv \lim_{t \rightarrow \infty} R, \quad (58)$$

we would expect from (41) and (43) that

$$\text{as } t^* \rightarrow \infty: \quad p^* - p_0^* \rightarrow \frac{1}{2}(p_h^* - p_0^*) \quad \text{for } 0 \leq r^* \leq R_f^* \quad (59)$$

and from (52) that

$$\text{as } t^* \rightarrow \infty: \quad p^* \rightarrow p_h^* \quad \text{for } r^* > R_f^*. \quad (60)$$

Recognizing (56), (59), and (60), we find that (57) gives [36]

$$\text{as } t^* \rightarrow \infty: \quad R^* \rightarrow R_f^* = \left(\frac{4 \Delta \rho g R_0^2}{3 \gamma^\infty} \right)^{1/2} R_b^{*2}. \quad (61)$$

Given R_b , we determine R_f by requiring (61) to be satisfied (since R_0 drops out of this equation). We identify $R_0 = R_f/R_f^*$.

For the sake of simplicity, let us define our characteristic speed

$$v_0 \equiv \frac{\mu}{\rho^{(C)} R_0}, \quad (62)$$

which means

$$N_{Re} = 1, \quad N_{We} = N_{ca} = \frac{\mu^2}{\rho^{(C)} R_0 \gamma^\infty}. \quad (63)$$

Note that we have not used this definition for v_0 or this definition for N_{Re} in scaling the Navier–Stokes equation to neglect inertial effects (assumption (viii)). The scaling argument required to suggest a priori under what circumstances inertial effects can be ignored would be different, based perhaps on the initial speed of displacement of one of the fluid–fluid interfaces calculated at the center of the film.

Our objective in what follows is to obtain a solution to (32) and (33) consistent with (41), (43) through (47), (50) through (55), and the second portion of assumption (xi). Given R_b , we determine R_f by requiring that, as $t^* \rightarrow \infty$ or just prior to the development of an instability and coalescence, (61) be satisfied; we identify $R_0 = R_f/R_f^*$. Note that, in addition to physical properties, only one parameter is required: R_b .

Integrating (33) twice consistent with (44), we find in view of (63)

$$v_r^* = \frac{1}{2} \left(\frac{h_0}{R_0} \right)^2 \frac{\partial \mathcal{P}^*}{\partial r^*} \left[z^{*2} - (h_1^* + h_2^*) z^* + h_1^* h_2^* \right]. \quad (64)$$

Substituting (64) into (32) and integrating once, we have

$$\begin{aligned} v_z^* = & -\frac{1}{2} \left(\frac{h_0}{R_0} \right)^2 \left\{ \left[\frac{\partial^2 \mathcal{P}^*}{\partial r^{*2}} + \frac{1}{r^*} \frac{\partial \mathcal{P}^*}{\partial r^*} \right] \right. \\ & \times \left[\frac{z^{*3}}{3} - \frac{1}{2} (h_1^* + h_2^*) z^{*2} + h_1^* h_2^* z^* \right] \\ & + \frac{\partial \mathcal{P}^*}{\partial r^*} \left[- \left(\frac{\partial h_1^*}{\partial r^*} + \frac{\partial h_2^*}{\partial r^*} \right) \frac{z^{*2}}{2} \right. \\ & \left. \left. + \left(\frac{\partial h_1^*}{\partial r^*} h_2^* + h_1^* \frac{\partial h_2^*}{\partial r^*} \right) z^* \right] \right\} - C(r^*), \quad (65) \end{aligned}$$

in which $C(r^*)$ is an as yet undetermined function of r^* .

With (64) and (65), Eq. (45) tells us ($i = 1, 2$)

$$\begin{aligned} \frac{\partial h_i^*}{\partial t^*} = & -\frac{1}{2} \left(\frac{h_0}{R_0} \right)^2 \left\{ \left[\frac{\partial^2 \mathcal{P}^*}{\partial r^{*2}} + \frac{1}{r^*} \frac{\partial \mathcal{P}^*}{\partial r^*} \right] \right. \\ & \times \left[\frac{1}{3} h_i^{*3} - \frac{1}{2} (h_i^* + h_2^*) h_i^{*2} + h_1^* h_2^* h_i^* \right] \\ & + \frac{\partial \mathcal{P}^*}{\partial r^*} \left[- \left(\frac{\partial h_1^*}{\partial r^*} + \frac{\partial h_2^*}{\partial r^*} \right) \frac{h_i^{*2}}{2} \right. \\ & \left. \left. + \left(\frac{\partial h_1^*}{\partial r^*} h_2^* + h_1^* \frac{\partial h_2^*}{\partial r^*} \right) h_i^* \right] \right\} - C(r^*) \quad (66) \end{aligned}$$

and the difference of these two expressions gives

$$\begin{aligned} \frac{\partial h^*}{\partial t^*} = & \left(\frac{h_0}{R_0} \right)^2 \left\{ \frac{1}{12} \left[\frac{\partial^2 \mathcal{P}^*}{\partial r^{*2}} + \frac{1}{r^*} \frac{\partial \mathcal{P}^*}{\partial r^*} \right] h^{*3} \right. \\ & \left. + \frac{1}{4} h^{*2} \frac{\partial h^*}{\partial r^*} \frac{\partial \mathcal{P}^*}{\partial r^*} \right\}. \quad (67) \end{aligned}$$

Taking the difference between (41) and (43), recognizing (56) and (63), and applying the appropriate expressions for the dimensionless mean curvatures H_i^* ($i = 1, 2$) as well as assumption (ii), we see

$$\begin{aligned} N_{ca} (p^* - p_0^*) + \frac{1}{R_b^*} & = N_{ca} (\mathcal{P}^* - \mathcal{P}_0^*) - N_{ca} [\Phi^{(C, \text{corr}) \infty^*} (h_2^*) \\ & \quad - \Phi^{(B, \text{corr}) \infty^*} (h_2^*)] + \frac{1}{R_b^*} \\ & = N_{ca} (\mathcal{P}^* - \mathcal{P}_0^*) + N_{ca} \Phi^{(B, \text{corr}) \infty^*} (h_2^*) + \frac{1}{R_b^*} \\ & = N_{ca} (\mathcal{P}^* - \mathcal{P}_0^*) - \frac{B^*}{h^{*4}} + \frac{1}{R_b^*} \\ & = -\frac{1}{2} \frac{h_0}{R_0} \frac{1}{r^*} \frac{\partial}{\partial r^*} \left(r^* \frac{\partial h^*}{\partial r^*} \right). \quad (68) \end{aligned}$$

In writing this, we have used the results of Slattery et al. [2, Section 2.2.7, exercise 2.2.7-2] in particular. We have also taken

$\gamma^* = 1$ by assumption (xiv), and we have defined

$$B^* \equiv \frac{R_0 B}{10\pi \gamma^\infty h_0^4}, \quad (69)$$

where, neglecting interactions with the gas phases A and B,

$$B \equiv (B^{(ACB)} - B^{(AC)} + B^{(CC)} - B^{(BC)}) = B^{(CC)}. \quad (70)$$

Inserting (68) into (67), we discover

$$\begin{aligned} -\frac{\partial h^*}{\partial t^{*'}} &= \frac{1}{3} h^{*3} \left(\frac{1}{r^{*3}} \frac{\partial h^*}{\partial r^*} - \frac{1}{r^{*2}} \frac{\partial^2 h^*}{\partial r^{*2}} + \frac{2}{r^*} \frac{\partial^3 h^*}{\partial r^{*3}} + \frac{\partial^4 h^*}{\partial r^{*4}} \right) \\ &+ h^{*2} \frac{\partial h^*}{\partial r^*} \left(-\frac{1}{r^{*2}} \frac{\partial h^*}{\partial r^*} + \frac{1}{r^*} \frac{\partial^2 h^*}{\partial r^{*2}} + \frac{\partial^3 h^*}{\partial r^{*3}} \right) \\ &+ \frac{8}{3} B^* \left[\frac{1}{r^*} \frac{1}{h^*} \frac{\partial h^*}{\partial r^*} + \frac{1}{h^*} \frac{\partial^2 h^*}{\partial r^{*2}} - \frac{2}{h^{*3}} \left(\frac{\partial h^*}{\partial r^*} \right)^2 \right], \end{aligned} \quad (71)$$

where

$$t^{*'} \equiv \frac{t\mu}{8\rho^{(C)} R_0^2 N_{ca}} \left(\frac{h_0}{R_0} \right)^3. \quad (72)$$

Note that, after an application of L'Hospital's rule with full recognition of (47), (50), and (51), we obtain

$$\text{limit } r^* \rightarrow 0: \quad -\frac{\partial h^*}{\partial t^{*'}} = \frac{8h^{*3}}{9} \frac{\partial^4 h^*}{\partial r^{*4}} + \frac{16}{3} \frac{B^*}{h^*} \frac{\partial^2 h^*}{\partial r^{*2}}. \quad (73)$$

Our first objective is to calculate the initial dependence of h^* upon radial position consistent with assumption (xi). Recognizing that the rate of thinning is independent of radial position at the initial time, we can use (71) and (73) to say at $t^{*' = 0}$

$$\begin{aligned} &\frac{8}{3} \left(\frac{\partial^4 h^*}{\partial r^{*4}} \right)_{r^*=0} + 16B^* \left(\frac{\partial^2 h^*}{\partial r^{*2}} \right)_{r^*=0} \\ &= h^{*3} \left(\frac{1}{r^{*3}} \frac{\partial h^*}{\partial r^*} - \frac{1}{r^{*2}} \frac{\partial^2 h^*}{\partial r^{*2}} + \frac{2}{r^*} \frac{\partial^3 h^*}{\partial r^{*3}} + \frac{\partial^4 h^*}{\partial r^{*4}} \right) \\ &+ 3h^{*2} \frac{\partial h^*}{\partial r^*} \left(-\frac{1}{r^{*2}} \frac{\partial h^*}{\partial r^*} + \frac{1}{r^*} \frac{\partial^2 h^*}{\partial r^{*2}} + \frac{\partial^3 h^*}{\partial r^{*3}} \right) \\ &+ 8B^* \left[\frac{1}{r^*} \frac{1}{h^*} \frac{\partial h^*}{\partial r^*} + \frac{1}{h^*} \frac{\partial^2 h^*}{\partial r^{*2}} - \frac{2}{h^{*3}} \left(\frac{\partial h^*}{\partial r^*} \right)^2 \right]. \end{aligned} \quad (74)$$

We require the result be consistent with (47), (50), and (46) in the form

$$\text{at } r^* = 1: \quad \frac{\partial h^*}{\partial r^*} = 0 \quad (75)$$

and with (52) expressed as

$$\text{as } r^* \rightarrow R_h^*: \quad \frac{1}{r^*} \frac{\partial}{\partial r^*} \left(r^* \frac{\partial h^*}{\partial r^*} \right) \rightarrow \frac{2}{R_b} \frac{R_0^2}{h_0}, \quad (76)$$

where p_h^* has been determined by (56) and p^* by (68).

In order to integrate a finite-difference form of (74), we replace (76) by

$$\text{at } r^* = 1: \quad \frac{\partial^2 h^*}{\partial r^{*2}} = C, \quad (77)$$

where C , which is the difference between the sum of the principal curvatures for interface 1 and the sum of the principal curvatures for interface 2, is a free parameter, the value of which will be determined shortly.

For each value of C , we can determine for a given value of B^* a tentative initial configuration of the film by integrating (74) consistent with (47), (51), (75), and (77). The dimensionless radial position at which the pressure gradient becomes negligible is tentatively identified as R_h , subject to later verification that assumption ii is still satisfied at this point.

Equation (71) can be integrated consistent with each of these tentative initial configurations, (47), (51), (25), and (26), the latter two boundary conditions first having been made dimensionless. Equation (46) permits us to identify R^* as a function of time; R_f^* is the value of R^* as $t^{*' \rightarrow \infty}$, which can be obtained from our numerical computation. We employed the Crank–Nicolson technique [37]; accuracy was checked by decreasing the time and space intervals. We used $\Delta r^* = 0.02$ and $\Delta t^{*' = 0.02$ to 0.05.

For a drop freely approaching a liquid–liquid interface under the influence of gravity and of a disjoining pressure that is greater than or equal to zero, R_b is measured and R_f is determined by [4,36,38]

$$\text{as } t^{*' \rightarrow \infty: \quad R \rightarrow R_f = \left(\frac{4}{3} \frac{\Delta \rho g}{\gamma^\infty} \right)^{1/2} (R_b)^2. \quad (78)$$

R_f^* is independent of the magnitude and sign of the disjoining pressure. There is no reason to believe that the initial film radius R_0 should be dependent upon the magnitude or sign of the disjoining pressure. It follows that R_f must also be independent of the magnitude and sign of the disjoining pressure. This implies that (78) is valid for the case of a negative disjoining pressure as well, in the limit as the time at which the film ruptures is approached.

Having determined R_f from (78) and $R_f^* = 1.1$ from our numerical computation, we can identify $R_0 = R_f/R_f^*$. From our numerical computation, we obtain $1/r^* [\partial/\partial r^* (r^* \partial h^*/\partial r^*)] = 12.58$ which allows us to determine h_0 from (76).

In addition to requiring that at time $t^{*' = 0}$ the thinning rate is independent of radial position, assumption (xi) demands that for $t^{*' > 0}$ the thinning rate at the center is always greater than the thinning rate at the rim, so long as the effects of any disjoining pressure are negligible. Our numerical computations indicate that, for sufficiently small $B^* > 0$, there is a minimum value of C such that the thinning rate at the center is always greater than the thinning rate at the rim in the early state of the thinning process where the effects of the disjoining pressure can be neglected. For each minimum value of C , there is a corresponding maximum value of h_0 for which the thinning rate at the center is always greater than the thinning rate at the rim for $t^{*' > 0$. We will choose this maximum value of h_0 as our initial film thickness at the center.

We must now check whether assumption (ii) is satisfied at R_h^* ; if it is satisfied here, it will be satisfied everywhere. It is desirable to choose R_h^* as large as possible, in order to make the pressure gradient at this point clearly negligible. But if R_h^* is assigned too large a value, assumption (ii) will be violated.

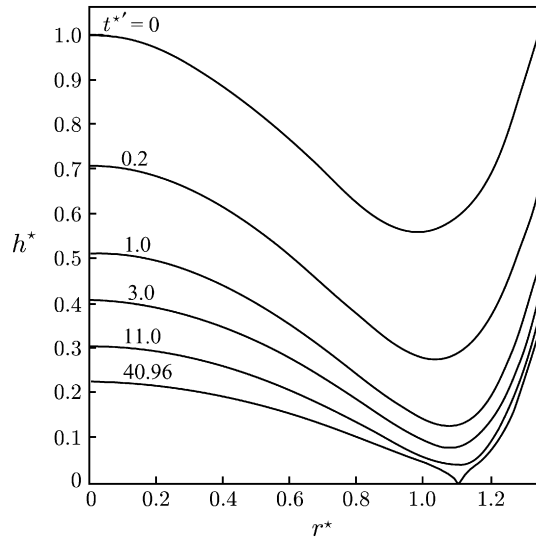


Fig. 4. Dimensionless film thickness, h^* , as a function of dimensionless radial position and dimensionless time for $R_h^* = 1.69$, $B^* = 10^{-7}$, $C = 5.05$.

If assumption (ii) cannot be satisfied by reducing R_h^* , C must be increased. For this reason, $h^*(r^*, t^{*'})$ is weakly dependent upon the bubble radius and the other physical parameters that enter (78).

We have from (43), (63), and (68)

$$\frac{1}{r^*} \frac{\partial}{\partial r^*} \left(r^* \frac{\partial h_2^*}{\partial r^*} \right) = -\frac{1}{2} \frac{1}{r^*} \frac{\partial}{\partial r^*} \left(r^* \frac{\partial h^*}{\partial r^*} \right) - \frac{R_0}{h_0} \frac{1}{R_h^*}. \quad (79)$$

Given h^* , we can integrate this consistent with (47) and (52) to determine h_2^* , the interface between phases C and D in Fig. 3. Having found h_2^* and h^* , we can compute h_1^* by difference.

Finally, we can examine assumption (iv) that the interfacial tension gradient required to achieve an immobile interface is very small. Given (64) and (68), and either (40) or (42), we can reason that

$$\frac{\partial \gamma^*}{\partial r^*} = -\frac{1}{2} \left(\frac{R_0}{h_0} \right)^2 h^* \left\{ \frac{1}{2} \frac{\partial}{\partial r^*} \left[\frac{1}{r^*} \frac{\partial}{\partial r^*} \left(r^* \frac{\partial h^*}{\partial r^*} \right) \right] + \frac{3B^*}{h^{*5}} \right\}. \quad (80)$$

This can be integrated consistent with

$$\text{at } r^* = R_h^*: \quad \gamma = 1, \quad (81)$$

which is in effect a definition for γ^∞ .

Fig. 4 shows the dimensionless film thickness h^* as a function of dimensionless radial position r^* and dimensionless time $t^{*'}$ for $R_h^* = 1.69$, $B^* = 10^{-7}$, $C = 5.05$. The dimensionless coalescence time t_c^* is identified as the dimensionless time at which the two interfaces touch or when $h^* = 0$.

2.1. Coalescence times

Let us define $t_c^{*'}$ as the dimensionless time at which the film thickness at the rim goes to zero or the dimensionless time at which the film ruptures. We will refer to this as our dimensionless coalescence time.

Our numerical computations express the relationship between the dimensionless coalescence time with dimensionless

Table 1
Experimental results for three different sizes of the bubble

$R_b \pm 0.01$ (mm)	$t_c \pm 0.1$ (s)	$R_b \pm 0.01$ (mm)	$t_c \pm 0.1$ (s)	$R_b \pm 0.01$ (mm)	$t_c \pm 0.1$ (s)
0.38	4.4	0.50	11.5	0.55	19.1
0.38	4.1	0.50	13.5	0.55	19.0
0.38	4.1	0.50	12.3	0.55	17.8
0.38	4.5	0.50	13.2	0.55	16.1
0.38	3.9	0.50	13.3	0.55	19.4

Hamaker constant as

$$t_c^{*'} = 2.5 \times 10^{-2} B^{*-0.46}. \quad (82)$$

In using this relationship, we recommend that (78) be employed to identify

$$R_0 = \frac{R_f}{1.1} = 1.05 \left(\frac{\Delta \rho g}{\gamma^\infty} \right)^{1/2} R_b^2. \quad (83)$$

The dimensionless mean curvature at $r^* = R_h^*$ was generated in our computation to be 12.58. This together with (76) and (83) fix the initial film thickness at the center:

$$h_0 = 0.175 \frac{\Delta \rho g R_b^3}{\gamma^\infty}. \quad (84)$$

In view of (72), (83), and (84), Eq. (82) may be rearranged as

$$t_c = 0.79 \frac{\mu (R_b)^{4.06} (\Delta \rho g)^{0.84}}{\gamma^\infty 1.38 B^{0.46}}. \quad (85)$$

Here μ is the viscosity of the continuous liquid phase, R_b the radius of the bubble, $\Delta \rho$ the density difference between the continuous phase and the drop or bubble, γ^∞ the interfacial tension, and B is the retarded Hamaker constant introduced in (70).

3. Experimental observations

A cylindrical container is partly filled with liquid hexadecane (99%, Sigma–Aldrich, Inc., St. Louis, USA). Air bubbles are released from the tip of a hypodermic needle near the bottom of the container. We photographed each bubble as it apparently came to rest at the hexadecane–air interface. Bubble diameters were measured in enlargements of these photographs, which also included a reference scale. Our measured coalescence time was the time that the bubble appeared to sit at the interface before disappearing. There were two reasons for the variation in the coalescence times for bubbles of nearly the same diameter. First, the instability leading to coalescence is not symmetrical as assumed in our theory. Second, there is the human response time in using a stopwatch. Table 1 shows the coalescence time t_c for three different bubble radii R_b .

4. Discussion

In order to use (85) to determine the coalescence time, we employed (13) from Görner and Pich [28] to estimate the retarded Hamaker constants B . We estimated the non-retarded Hamaker constant for hexadecane $A = 5.23 \times 10^{-20}$ J [39, Table 4], the surface tension $\gamma^\infty = 27.6 \times 10^{-3}$ N/m [40],

Table 2
Comparison between experimental observation $t_c^{(\text{exp})}$ (Table 1) and the prediction $t_c^{(\text{theo})}$ of (85)

R_b (mm)	$t_c^{(\text{exp})}$ (s)	$t_c^{(\text{theo})}$ (s)
0.38 ± 0.01	3.8 to 4.6	3.72 to 4.60
0.50 ± 0.01	11.4 to 13.6	11.6 to 13.7
0.55 ± 0.01	16.0 to 19.5	17.2 to 20.0

the density $\rho = 773 \text{ kg/m}^3$, and the viscosity $\mu = 3.34 \times 10^{-3} \text{ kg m}^{-1} \text{ s}^{-1}$ [41]. Görner and Pich [28] did not define λ_L , simply referring to it as the “London wavelength.”

In discussing retarded dispersion forces, Hirschfelder et al. [42, pp. 963 and 967] introduce the “dominant wavelength” λ , noting that it and the corresponding dominant frequency must be determined empirically, although they do estimate λ “... is of the order of 1200 \AA ...” This should be compared with the estimate by Overbeek [29, p. 266] of “... 1000 \AA or thereabouts ...” or 1030 \AA an extrapolation from the visible spectrum to the UV absorption frequency [39] and quoted by Israelachvili [16, p. 200].

On the basis of this single study, we recommend using the largest wavelength from the IR spectrum [43] when estimating the retarded Hamaker constant B using (85). With this decision, we have the comparison between theory and experiment in Table 2. The range in predicted coalescence times is attributable to the uncertainty in the measurement of the bubble radius.

5. Conclusions

- (1) This appears to be the first time that (85) has been tested, since to our knowledge no comparable experimental data have been reported previously for bubble coalescence.
- (2) This comparison between theory and experiment lends further support for the theory of Slattery et al. [10], since no adjustable parameters are required.
- (3) This is the first test of (13) from Görner and Pich [28], which relates the retarded and non-retarded Hamaker constants.

Acknowledgment

The authors appreciate the help given by Yongzhe Tian in setting up the experiments.

Appendix A. Notations

Roman symbols

- $A, A^{(AB)}$ non-retarded Hamaker constant between species A and B
- \mathbf{b} body force per unit mass
- $\mathbf{b}^{(A, \text{corr})}$ body force per unit volume at a point in phase A . This is introduced to correct for the use of bulk material behavior in the interfacial region
- $\mathbf{b}^{(A, \text{corr})\infty}$ body force per unit volume at a point in phase A . This is introduced to correct for the use of surface tension on a dividing surface

- $B, B^{(AB)}$ retarded Hamaker constant between species A and B
- $B^{(ACB)}$ retarded Hamaker constant for species A and B interacting across an interface phase C
- B^* dimensionless retarded Hamaker constant introduced in (69)
- h film thickness
- h_1 configuration of the fluid–fluid interface
- h_2 configuration of the drop–fluid interface
- h_0 film thickness at $t = 0$ and $r = 0$
- H_i mean curvatures of the interfaces
- N_{Bo} Bond number defined by (27)
- N_{ca} capillary number defined by (30)
- N_{Re} Reynolds number defined by (30)
- N_{We} Weber number defined by (30)
- \mathcal{P}^* dimensionless modified pressure defined in (29)
- \mathbf{P} projection tensor [2, Section A.3.2]
- p_0 pressure within phase B
- p_h hydrostatic pressure
- r cylindrical coordinate
- r^* dimensionless cylindrical coordinate
- R rim radius of the drop
- R_0 rim radius of the drop at $t = 0$
- R_b radius of the drop
- R_f dimple radius as $t \rightarrow \infty$
- R_h radial position where the pressure within the liquid film approaches the local hydrostatic pressure in the neighborhood of the bubble
- t^* dimensionless time
- t_c predicted coalescence time defined by (85)
- \mathbf{T} bulk stress tensor using bulk description of material behavior
- $\mathbf{T}^{(I)}$ stress tensor using real description of material behavior
- $\mathbf{T}^{(I, \text{bulk})}$ stress tensor using bulk description of material behavior, corrected for intermolecular forces from the adjoining phase
- $\mathbf{T}^{(I, \text{bulk})\infty}$ stress tensor using bulk description of material behavior, corrected for intermolecular forces from the adjoining phase when the surface tension is introduced to the dividing surface
- $\mathbf{v}^{(I)}$ velocity using real description of material behavior
- $\mathbf{v}^{(I, \text{bulk})}$ velocity using bulk description of material behavior, corrected for intermolecular forces from the adjoining phase
- \mathbf{v} velocity vector
- v_0 characteristic speed

Greek letters

- $\xi^{(\alpha)}$ unit normal to the interface pointing into phase α
- γ surface tension (or energy)
- γ^∞ equilibrium surface tension
- $\gamma^{(AC)}$ surface tension between phases A and C
- μ bulk viscosity of the liquid film
- $\rho^{(I)}$ bulk density using real description of material behavior

- $\rho^{(l, \text{bulk})}$ bulk density using bulk description of material behavior, corrected for intermolecular forces from the adjoining phase
- $\rho^{(\alpha)}$ density in phase α
- $\rho^{(\sigma)}$ surface density on a dividing surface
- $\Delta\rho$ density difference between liquid film and the drop
- λ dominant wavelength
- ϕ_{nr} non-retarded point-to-point potential
- ϕ_r retarded point-to-point potential
- $\Phi^{(A, \text{corr})}$ net correction for intermolecular potential at a point in phase A
- $\Phi^{(A, \text{corr})\infty}$ net correction for intermolecular potential at a point in phase A when the surface tension is introduced to the dividing surface

References

- [1] L.G. Leal, *Phys. Fluids* 16 (4) (2004) 1833–1851.
- [2] J.C. Slattery, L.M.C. Sagis, E.S. Oh, *Interfacial Transport Phenomena*, second ed., Springer-Verlag, New York, 2007.
- [3] P.S. Hahn, J.C. Slattery, *AIChE Symp. Ser.* 82 (252) (1986) 100–118.
- [4] C.Y. Lin, J.C. Slattery, *AIChE J.* 28 (1982) 786–792.
- [5] P.S. Hahn, J.D. Chen, J.C. Slattery, *AIChE J.* 31 (1985) 2026–2038.
- [6] P.S. Hahn, J.C. Slattery, *AIChE J.* 31 (1985) 950–956.
- [7] D. Li, J.C. Slattery, *AIChE J.* 34 (1988) 862–864.
- [8] D.M. Li, *J. Colloid Interface Sci.* 181 (1996) 34–44.
- [9] D.M. Li, *Chem. Eng. Sci.* 51 (14) (1996) 3623–3630.
- [10] J.C. Slattery, E.-S. Oh, K. Fu, *Chem. Eng. Sci.* 59 (2004) 4621–4635.
- [11] P. Hein, *Z. Phys. Chem. (Munich)* 86 (1914) 385–410.
- [12] C.A. Winkler, O. Maass, *Can. J. Phys.* 9 (1933) 613–629.
- [13] O. Maass, *Chem. Rev.* 23 (1938) 17–28.
- [14] R.L. McIntosh, J.R. Dacey, O. Maass, *Can. J. Res. Sect. B* 17 (1939) 241–250.
- [15] H.B. Palmer, Ph.D. thesis, University of Wisconsin, 1952.
- [16] J.N. Israelachvili, *Intermolecular and Surface Forces*, second ed., Academic Press, New York, 1991.
- [17] W.R. Bowen, F. Jenner, *Adv. Colloid Interface Sci.* 56 (1995) 201–243.
- [18] R.S. Allan, G.E. Charles, S.G. Mason, *J. Colloid Sci.* 16 (1961) 150–165.
- [19] G.D.M. MacKay, S.G. Mason, *Can. J. Chem. Eng.* 41 (1963) 203–212.
- [20] A. Vrij, *Discuss. Faraday Soc.* 42 (1966) 23–33.
- [21] I.B. Ivanov, B. Radoev, E. Manev, A. Sheludko, *Trans. Faraday Soc.* 66 (1970) 1262–1280.
- [22] K.A. Burrill, D.R. Woods, *J. Colloid Interface Sci.* 42 (1973) 15–34.
- [23] J.D. Chen, P.S. Hahn, J.C. Slattery, *AIChE J.* 30 (1984) 622–630.
- [24] H.B.G. Casimir, D. Polder, *Phys. Rev.* 73 (4) (1948) 360–372.
- [25] W.B. Russel, D.A. Saville, W.R. Schowalter, *Colloidal Dispersions*, Cambridge Univ. Press, Cambridge, 1989.
- [26] J. Mahanty, B.W. Ninham, *Dispersion Forces*, Academic Press, New York, 1976.
- [27] A.D. Zimon, *Adhesion of Dust and Powder*, second ed., Consultants Bureau, New York, 1982.
- [28] P. Görner, J. Pich, *J. Aerosol Sci.* 20 (7) (1989) 735–747.
- [29] J.Th.G. Overbeek, in: H.R. Kruyt (Ed.), *Colloid Science*, vol. 1, Elsevier, Amsterdam, 1952, pp. 245–277.
- [30] A. Sheludko, *Adv. Colloid Interface Sci.* 1 (1967) 391–464.
- [31] C.Y. Lin, J.C. Slattery, *AIChE J.* 28 (1982) 147–156.
- [32] T.D. Hodgson, D.R. Woods, *J. Colloid Interface Sci.* 30 (1969) 429–446.
- [33] E.S. Oh, J.C. Slattery, J.R. Walton, *J. Appl. Mech.* 73 (2006) 792–798.
- [34] J.C. Slattery, *Advanced Transport Phenomena*, Cambridge Univ. Press, New York, 1999.
- [35] K. Fu, R.L. Robinson, J.C. Slattery, *Chem. Eng. Sci.* 59 (2004) 801–808.
- [36] D.C. Chappellear, *J. Colloid Sci.* 16 (1961) 186–197.
- [37] G.E. Myers, *Analytical Methods in Conduction Heat Transfer*, McGraw-Hill, New York, 1971.
- [38] H.M. Princen, *J. Colloid Sci.* 18 (1963) 178–195.
- [39] D.B. Hough, L.R. White, *Adv. Colloid Interface Sci.* 14 (1980) 3–41.
- [40] J.J. Jasper, R.E. Kerr, G. Frederick, *J. Am. Chem. Soc.* 75 (21) (1953) 5252–5254.
- [41] R.C. Weast (Ed.), *CRC Handbook of Chemistry and Physics*, 68th ed., CRC Press, Boca Raton, 1987.
- [42] J.O. Hirschfelder, C.F. Curtiss, R.B. Bird, *Molecular Theory of Gases and Liquids*, Wiley, New York, 1954, corrected with notes added 1964.
- [43] D.R. Lide, *Properties of Organic Compounds*, web 6.0 edition, CRC Press, Boca Raton, 2005.